

Analysis of flood inundation in ungauged basins based on multi-source remote sensing data

Wei Gao  · Qiu Shen · Yuehua Zhou · Xin Li

Received: 10 September 2017 / Accepted: 22 January 2018 / Published online: 9 February 2018
© Springer International Publishing AG, part of Springer Nature 2018

Abstract Floods are among the most expensive natural hazards experienced in many places of the world and can result in heavy losses of life and economic damages. The objective of this study is to analyze flood inundation in ungauged basins by performing near-real-time detection with flood extent and depth based on multi-source remote sensing data. Via spatial distribution analysis of flood extent and depth in a time series, the inundation condition and the characteristics of flood disaster can be reflected. The results show that the multi-source remote sensing data can make up the lack of hydrological data in ungauged basins, which is helpful to reconstruct hydrological sequence; the combination of MODIS (moderate-resolution imaging spectroradiometer) surface reflectance productions and the DFO (Dartmouth Flood Observatory) flood database can achieve the macro-dynamic monitoring of the flood inundation in ungauged basins, and then the differential technique of high-resolution optical and microwave images before and after floods can be used to calculate flood extent to reflect spatial changes of inundation; the monitoring algorithm for the flood depth combining RS and GIS is simple and easy and can quickly calculate the depth with a known flood extent that is obtained from remote sensing images in ungauged basins. Relevant

results can provide effective help for the disaster relief work performed by government departments.

Keywords Flood disaster · Inundation · Remote sensing monitoring · Ungauged basins

Introduction

Floods are among the most expensive natural hazards experienced in many places of the world and can result in heavy losses of life and economic damages (Awadallah and Tabet 2015). In the past few decades, economic and insured losses have dramatically increased due to severe floods, and intangible impacts, for example, the loss of life, memorabilia, health and cultural damages, and stress or psychological trauma, have been considered even more serious than the loss of property (Aronica et al. 2012; Khan et al. 2011). To minimize the repercussions of floods, scientific and effective detections need to be conducted to fully grasp the disaster characteristics, to assist in risk assessment, and to develop various effective relief countermeasures, which has important practical significance (Li et al. 2014; Plate 2002). In the detection of floods, flood extent, depth, and duration are main monitoring elements.

Flood extent forms the basis of all studies, and the acquisition of this information includes flood water extraction and inundated area calculation (Huang et al. 2012). Determining the flood extent from in situ observations and on-the-ground efforts is costly,

W. Gao (✉) · Q. Shen · X. Li
Faculty of Information Engineering, China University of
Geosciences, Wuhan, China
e-mail: cuggaowei@hotmail.com

Y. Zhou
Wuhan Regional Climate Centre, Wuhan, China

impractical, and can be inaccurate; further, current processes cannot meet the needs of modern flood prevention. Remote sensing can rapidly collect relevant information concerning ground objects with the advantages of macroscopic scale, high efficiency, real-time performance, and dynamicity, and it is often used in environmental monitoring, such as drought and flood monitoring (Shen et al. 2017; Huang et al. 2016; Qian et al. 2016; Liang et al. 2016; Liang et al. 2015; Du et al. 2012). Nowadays, remote sensing has gradually become the primary means and is playing an increasingly important role in the flood monitoring, especially in mapping inundation (Wolski et al. 2017). Different types of remote sensing data sources have different features in disaster information extraction: spaceborne and airborne visible and near infrared imagery can provide consistent, rapid, and repeated measurements of flooding through time over large geographic areas; microwave radar is sensitive to water and capable of all-weather day/night observations, which allows for the discrimination between land and smooth open water surfaces over large scales. The data is attainable at medium-high resolution (e.g., 5–25 m), rendering these systems extremely useful for flood detection (Ahamed and Bolten 2017). Among microwave data, synthetic aperture radars (SARs) are the most representative, and their potential is tested in lots of locations, improving our understanding of flood inundation (Zeng et al. 2015). However, due to bad weather, such as rains or clouds during floods, and the limited spatial-temporal resolution of the images from single satellite sensor, collaborative observations of multi-source remote sensing data have a unique advantage of obtaining more information allowing for an accurate and detailed description of disaster characteristics, which can also improve the accuracy and reliability of water recognition and extraction. There have been a lot of studies on monitoring flood extent with the combination of multi-source data. Huang et al. (2014) integrated time-series river flow data and MODIS images to map inundation dynamics at large river basin scale on both temporal and spatial dimensions; Powell et al. (2014) discussed the usage of the Normalized Difference Vegetation Index (NDVI) of time series obtained from Landsat, MODIS, and AVHRR (Advanced Very High Resolution Radiometer) to reflect the flood extent in macrophyte-dominated floodplain wetlands. Nakmuenwai et al. (2017) extracted the inundated areas from multi-temporal dual-polarization RADARSAT-2 images of the 2011 central Thailand flood, and the

extracted results were validated using high-resolution optical images from the GeoEye-1 and ThaiChote-1 satellites and water elevation data from gaging stations.

Flood depth is also an important factor used to measure the severity and assess the damage of floods. The traditional method of water depth monitoring is to use sounding equipment (such as echo sounders and multi-beam sonar) and positioning equipment (such as sextants and radar positioning instruments) installed on the ships to measure the target water (Zhao et al. 2016). In this way, underwater topography data of the studied area can be obtained. Due to the complex environmental conditions and wide ranges of studied areas, there are several drawbacks to the above method, including synchronization, economy, periodicity, flexibility, and macroeconomics of the data. With the rapid development of “3S” technology, their applications to the measurement of water depth have increased and obtain good results, which can be divided into water depth inversions based on remote sensing, water depth simulations based on hydrological hydraulic models, and water depth measurements combining RS and GIS. Water depth inversions based on remote sensing include active inversions (e.g., microwave radar and airborne laser radar) and passive inversions (e.g., visible light remote sensing). Sandidge and Holyer (1998) used data from the airborne visible/infrared imaging spectrometer (AVIRIS) in a neural network system to establish quantitative, empirical relationships between one of these parameters, depth, and remotely sensed spectral radiance; Calkoen et al. (2001) described the Bathymetry Assessment System (BAS) in detail and constructed accurate depth maps from radar images and a limited number of echo soundings. In the water depth simulations based on hydrological hydraulic models, distributed hydrological models are commonly used (Zhang and Wang 2009). The water depth measurements combining RS and GIS are often used in calculating flood depth with a known extent. Using the GIS method to obtain the flood depth usually requires the support of the Digital Elevation Model (DEM), and the flood depth is determined by the water surface elevation and the ground elevation. Yi et al. (2005) proposed an algorithm to calculate the depth distribution within an inundated region extracted from remote sensing imagery. The algorithm combined the flood region with DEM and acquired a smooth elevation distribution in the flood borderlines after efficiently controlling for errors in the inadequate precision of the imagery processing and DEM itself. After

assuming the water surface in the inundated area to be an inclining plane, the depth distribution within the boundary could be computed with bilinear interpolation. Several studies have also tried to map flood depth using a combination of remote sensing images and DEM by applying a series of cross section profiles along the centerline of a river reach, which requires a large amount of manual work in order to identify the centerlines and cross sections (Zwenzner and Voigt 2009; Matgen et al. 2007).

However, some flood prone areas are located outside the hydrological monitoring network, without effective information to reconstruct sequence of hydrological elements. Thus, for the ungauged basins, especially those basins with few gauged stations and complicated terrain conditions, remote sensing is the only alternative to calculate the flood extent and depth to make up for the lack of discrete field sampling points (Papa et al. 2008). Further, in the course of flood disaster, there are two aspects worth considerations: one is that the complex weather conditions, such as rains, clouds, and fogs, make single remote sensing data source not achieve the whole monitoring; another is that fast time-serial monitoring is required for disaster's frequent occurrence, large intensity, and short duration, including macroscopic and specific monitoring. Therefore, remote sensing data from different satellites or sensors, with different resolutions, should be used to achieve comprehensive understanding on floods. Some scholars have made some relevant attempts. In this paper, we perform near-real-time flood detection with flood extent and depth based on multi-source remote sensing data in ungauged basins. Via spatial distribution analysis of flood extent and depth in a time series, the inundation state and the characteristics of flood disaster can be reflected, which provides effective help for the disaster relief work performed by government departments.

Materials and methods

General description of the study area

The Jushui River is a tributary of the Yangtze River located in Hubei Province, China. It flows from north to south and runs through Macheng, Xinzhou, and Tuanfeng. The total length of the mainstream is 170.4 km, with a basin area of 4367.6 km². There are three types of topography in the basin: mountains, hills,

and plains, coupled with a sloping terrain from northeast to southwest. A hydrological station, the Liuzi Port, is located at the junction of the middle and lower reaches: the upper reaches are located between the source of the river and the bridge in Macheng, with a river width of 10–280 m; the middle reaches are located between the bridge in Macheng and the Liuzi Port, with a river width of 280–400 m; and the lower reaches are located between the Liuzi Port and the outlet of the river, with a river width of 800–1000 m. The middle and lower reaches are densely populated, and there are densely planted forests in the mountains and cultivated land on the plains. Influenced by the hot and humid air masses of the Pacific and the cold air masses of Siberia, rainstorms in the basin occur from May to July, accounting for 70% of the annual rainfall. When floods occur in the upstream of the river, water flows to the downstream rapidly, which causes the dykes of the downstream to collapse and threatens the lives and property of the local people. From June 30 to July 4, 2016, a wide range of continuous heavy rain happened in the middle and lower reaches of the Yangtze river and had caused severe floods in the Jushui Basin, including the collapse of houses, the destruction of farmlands, and serious damages to infrastructures in Macheng, Xinzhou, and Tuanfeng. This paper focuses on floods at this time period in the lower reaches of the Jushui Basin. The location of the Jushui River is showed in Fig. 1.

Data available

The available remote sensing data can be categorized into four types: (a) optical satellite images, (b) the Dartmouth Flood Observatory (DFO), (c) microwave radar, and (d) topography missions. Table 1 presents the detailed information of these data sources.

Optical satellite images

Inundation detection using optical satellite images is possible because water bodies are easily identifiable for their low reflectance. To perform remote sensing monitoring of floods in the Jushui Basin, optical satellite images need to have a higher spatial resolution and temporal resolution to effectively identify water bodies and to obtain high frequency data to analyze the water variation characteristics. In many satellite remote sensors, MODIS is an ideal data source due to its high space-time resolution and spectral resolution, as well as its wide coverage, accurate radiation calibration,

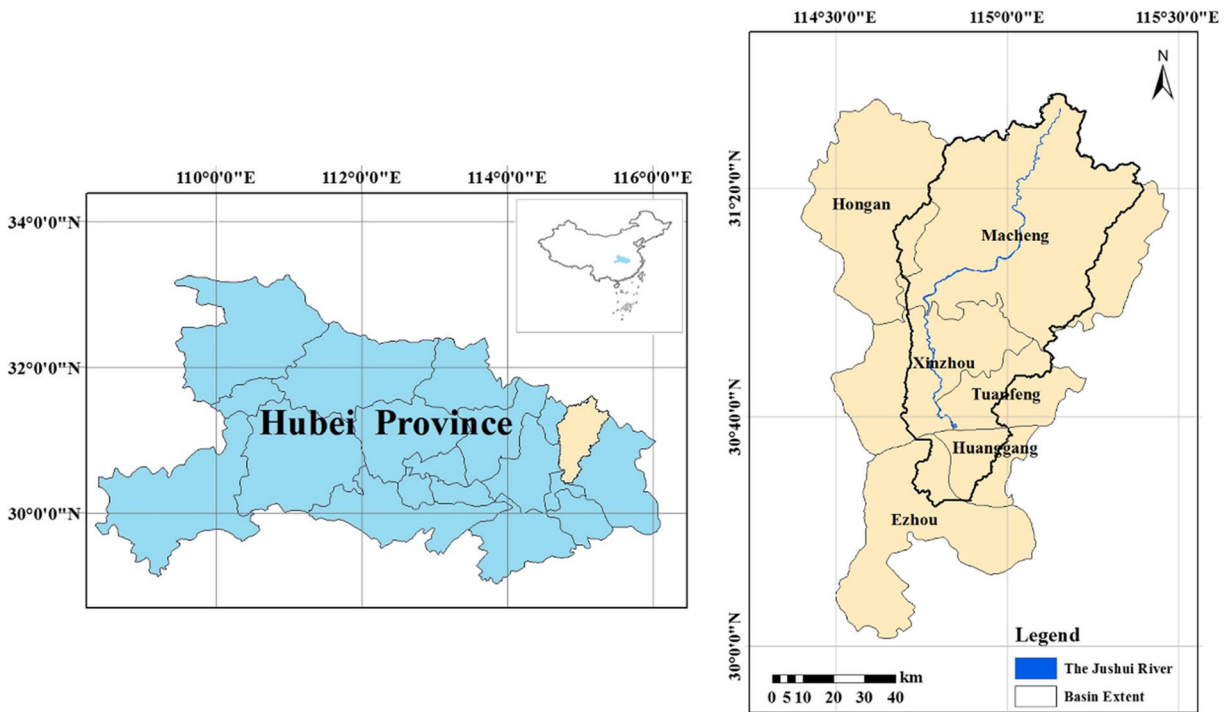


Fig. 1 Spatial distribution of study area in China

and free access. MODIS sensor on the Aqua and Terra satellites observes the Jushui Basin twice daily at approximately 10:30 AM and 1:30 PM local time. Even though the local weather conditions during the monsoon season in the basin can be persistently cloudy, clear MODIS images can be used to extract inland water body information and to determine flood extents rapidly and

effectively (Zhang et al. 2015). In July 2016, the water level in the Jushui River dramatically increased due to heavy rainfall and it caused dikes in Xinzhou to break. Therefore, focusing on the lower reaches of the Jushui Basin, this article used MODIS surface reflectance productions MOD09GQ and MYD09GQ as data sources of the real-time observations, downloading the red and

Table 1 Data used for this study

Type	Information	Source	Spatial resolution	Date acquired
DEM	ASTGTM2_N30E114	Chinese Geospatial Data Cloud	30 m	
Remote sensing image	MODIS surface reflectance productions	NASA web	250 m	01/07/2016–20/07/2016
	GF-1 WFV3	China Centre For Resources Satellite Data and Application	16 m	14/06/2016
	Sentinel-1 SAR	Sentinel web		05/07/2016
	Landsat-7 ETM+	Chinese Geospatial Data Cloud	30 m	08/07/2016
	GF-1 WFV4	China Centre For Resources Satellite Data and Application	16 m	09/07/2016
Inundated region	Daily surface water records of flood	The United States Dartmouth College		01/07/2016–20/07/2016
Boundary	Vector boundary of basin	Hubei Province Meteorological Bureau		

near infrared bands (620–670 nm and 841–876 nm, respectively) from day 183 to day 202 in 2016.

There were similar flooding situation between Landsat-7 ETM+ (Enhanced Thematic Mapper Plus), GF-1 WFV4 (Wide Field View) satellite images of relatively higher resolution and MODIS surface reflectance productions during the same period, so Landsat-7 ETM+, GF-1 WFV4 satellite images were used to verify the accuracy of the water extraction. Of these, the Landsat-7 satellite has had a faulty scan line corrector since May 2003. Therefore, all the retrieved images have wedge-shaped gaps (regular missing/bad lines) on both sides of each scene, resulting in data loss of approximately 22%. In this paper, the stripe in the Landsat-7 ETM+ image was repaired with a plug-in unit called `landsat_gapfill` and the fusion of the multispectral and panchromatic band obtained a true color image with high resolution. The GF-1 satellite launched in 2013 is the star of the Chinese high-resolution earth observation system. It has two panchromatic cameras with 2 m resolution, two multispectral cameras with 8 m resolution, and four multispectral cameras with 16 m resolution. These sensors achieve a perfect combination of high spatial resolution and high time resolution and provide important services and decision support for modern Chinese agriculture, disaster prevention and mitigation, resources, environment, public security, and other important fields. Before used to verify the accuracy of the water extraction by MODIS, the Landsat-7 ETM+ and GF-1 WFV4 satellite images require pretreatments for the radiation calibration and the FLAASH (the Fast Line-of-Sight Atmospheric Analysis of Spectral Hypercubes) atmospheric correction.

The calculation of flood extent needs to use the differential technique of the inundated water body and the background water body. In early June 2016, there was no heavy rainfall in a large area of the Jushui Basin; therefore, the water body at this time could be regarded as the background water body without inundation conditions prior to the study period. This paper selected the GF-1 WFV3 image on June 14 as the original water data to identify and quantify the spatial distribution and changes of the flood extent.

The DFO flood database

The DFO flood database provided by the United States Dartmouth College (Hanover) Research Center is a long time series contour map of floods and uses an algorithm

applied to near real-time MODIS imagery to detect surface water at 500 m resolution (Ahamed and Bolten 2017). These surface water records are comprehensive records of satellite-observed changes in the Earth's inland surface waters. Recent GIS data (daily surface water information) from the automated MODIS-LANCE NRT processor can be found at http://csdms.colorado.edu/pub/flood_observatory/MODISlance/. The Flood Observatory website provides recent and historical archives of global flooding detected by the algorithm, as well as other flood information such as discharge estimates (<http://floodobservatory.colorado.edu/http://floodobservatory.colorado.edu/>). An accuracy assessment of this product on a global scale is still ongoing (Nigro et al. 2014).

SAR data

A major difficulty in flood detection is to find cloud-free images during, or as close as possible to, the flood event. SAR can provide information concerning the surface roughness, terrain, humidity conditions, and vegetation growth. Due to the rugged topography, land surfaces in SAR images become submerged areas from never-flooded areas when floods occur, and the soil moisture approaches saturation. When a land surface is completely covered by flood water, the image tone turns to dark gray or black. Therefore, SAR can be used for an indirect estimation of the water elevation and flooded areas, further reflecting the flood situation. A single Sentinel-1 satellite revisits a location every 12 days with a spatial resolution of 20 m and can provide effective image information of floods for free; therefore, it was chosen as the microwave source for the flood extent monitoring in this article. Sentinel-1 data was processed via multilooking, single image filtering, geocoding, and radiometric calibration and then a threshold was set to extract the water body.

Topographic information

A DEM is a physical model of the ground using a numerical array to represent a set of orderly ground elevations; it is also a branch of the Digital Terrain Model (DTM). The DEM in this paper was downloaded

from the Chinese Geospatial Data Cloud and had a spatial resolution of 30 m.

Analysis of flood inundation in ungauged basins

Given the above, the proposed approach adapts and applies a number of different techniques. The undertaken methodology is summarized in the following steps and illustrated in Fig. 2:

- a. Collection of all available remote sensing data;
- b. Determination of the flood extent in the lower reaches of the Jushui Basin during the flooding event in July 2016; and
- c. Determination of the flood depth in the lower reaches of the Jushui Basin during the flooding event in July 2016.

The above steps are detailed below. Because calibration data were unfortunately unavailable, the first step in the methodology was to compare the remote sensing information sources to obtain a robust and realistic estimate of the floods. The advantages of the optical satellite images were their good resolution

and their well-acknowledged capabilities in land use determination including water bodies (Awadallah and Tabet 2015). However, they were only available on a daily basis and were very sensitive to cloud coverage, which caused non-effective detection. Conversely, the SAR information relied on passive microwave data and was less sensitive to clouds. Therefore, it had a higher probability of capturing the maximum daily flooding event.

The second and third steps in the methodology were undertaken to achieve an understanding of the flooding event in the Jushui Basin and to lay a foundation for disaster assessment.

The extraction of flood extent based on multi-source remote sensing data

For the flood water body extraction, domestic and foreign scholars have proposed many methods, including density slicing, image classification, single-band threshold method, multi-band spectral relationship method, and water indices. The Normalized Difference Water Index (NDWI) and the Modified Normalized Difference Water Index (MNDWI) are common water indices, and they are developed explicitly with the purpose of

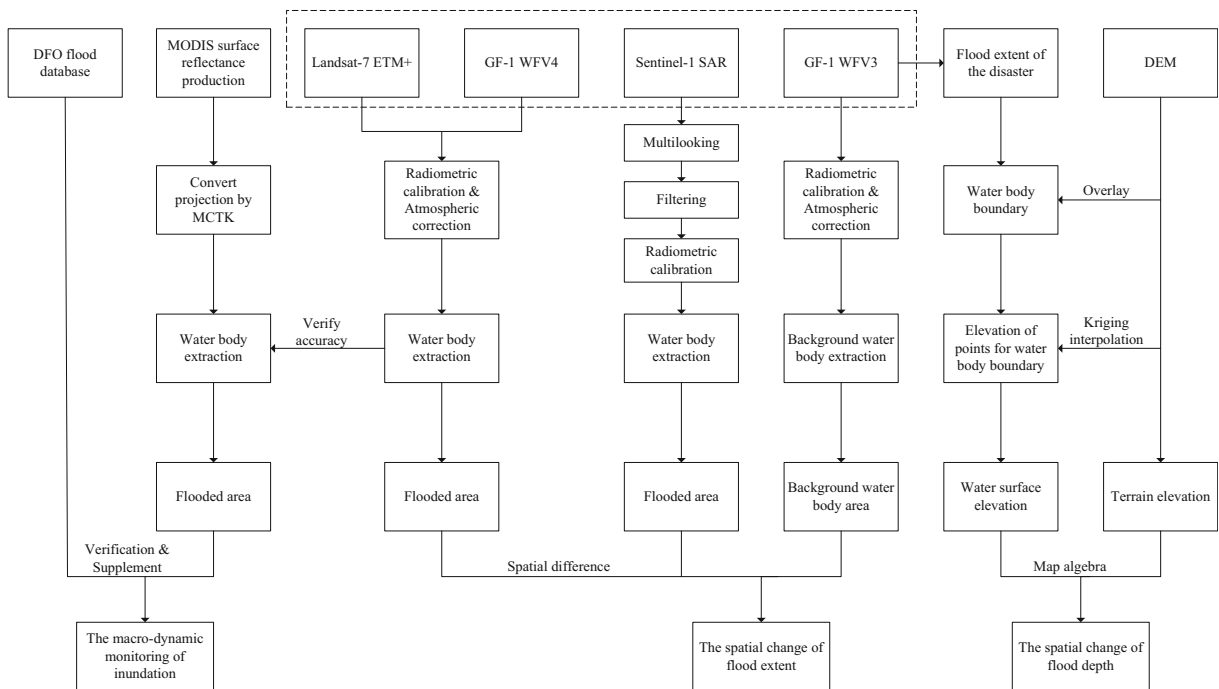


Fig. 2 Flowchart of the method

mapping open water bodies (McFeeters 1996; Xu 2006). Besides, some vegetation indices, like the Difference Vegetation Index (DVI), the Ratio Vegetation Index (RVI), and the Normalized Difference Vegetation Index (NDVI), are also used to extract water body. NDVI is adopted in inundation mapping for its sensitivity to the presence of open water or vegetated water in the radiometer's field of view. Because water reflectance in the red band is higher than that in the near infrared band, contrary to the vegetation reflectance in these two bands, their ratio can be used to enhance the contrast between water and land. The NDVI value of water is less than 0, while the NDVI value of vegetation and bare soil is greater than 0. By setting an appropriate threshold, water can be extracted from soil and vegetation. Therefore, considering the characteristics of vegetation and water in the study area, the vegetation index NDVI, which is simple, easy, and efficient, is chosen as an index for water extraction.

It was difficult to determine the inspection precision of water extraction by MODIS in the Jushui Basin due to the difficulty of field verification and the long inspection cycle in such a small basin. Therefore, remote sensing images with relatively higher resolution, including the Landsat-7 ETM+, GF-1 WFV4 images, were adopted to verify the precision of the water extraction by MODIS, which was time-saving, energy-saving, and made up for the lack of high efficiency field validation techniques (Huang et al. 2013). Specifically, by using the minimum adjacent method in the resampling, relatively high-resolution data were transformed to a unified resolution. This was done because there was a scale effect in the geographical spatial data. At different spatial scales, the error between the real area and the calculated area corresponded to the complexity of the land use under the same scale (resolution) (Liu et al. 2001). After resampling, the relatively high-resolution data was compared with low-resolution data at the same scale. In addition, because some of the MODIS images could not monitor the flood extent size due to clouds, the profiles of the DFO flood database were able to complete the verification and supplement the water-flooded area.

However, the MODIS surface reflectance productions and DFO flood database were only suitable for macro-dynamic monitoring, and the inundation details in the Jushui Basin during the flood could not be well reflected, because these data were unable to obtain accurate information concerning the spatial variation

of the inundated area. Therefore, a GF-1 WFV3 image on June 14 was used as the background water without inundation condition before the flood, and the Landsat-7 ETM+, GF-1 WFV4, and Sentinel-1 SAR data were resampled to a resolution of 30 m to calculate the spatial differences for the flood extents in order to understand the spatial changes of inundation.

The calculation of flood depth based on multi-source remote sensing data

The flood depth is indispensable to flood disaster assessments and is an important index to evaluate disaster losses. Using the GIS method to calculate the flood depth usually requires the support of DEM. The difference between the water surface elevation and the ground elevation is treated as the flood depth:

$$D = E_w - E_g \quad (E_w > E_g)$$

where D is the flood depth; E_w is the water surface elevation; and E_g is the ground elevation (Huang et al. 2012). The water surface can be horizontal, an inclined plane, or even a complex curved surface; therefore, calculations of the surface elevation must first determine the extent and form of the water surface. Influenced by the topography and the water depth, a static water surface should have a complex curved surface, which is difficult to describe with an equation, and requires big computation. Therefore, the curved surface is simplified as a plane when calculating the flood depth, and some practices have proved that this approximation can meet the application requirements. In this paper, flooded areas were extracted via remote sensing images; these areas may be irregular or may be broken into multiple independent water surfaces. Therefore, the water surface was simplified into oblique planes (including horizontal planes). Then, the oblique planes and DEM were combined to obtain the elevation points of the flood boundary. The elevation of the water surface could be obtained by interpolating these elevation points. A Kriging interpolation was used to manage this process with Geostatistical Analyst in ArcGIS. Finally, the water depth was calculated with the spatial difference between the water surface elevation and the terrain elevation.

The most rigorous method to evaluate the output surface quality is to compare observations with predicted values. Typically, people need to go to the research area to collect independent validation datasets. Another

way is to use the Create Subsets module to divide the sampling points into training samples and test samples. Because the field validation in the Jushui Basin was complex, the second way was used. To deal with the uncertainty in the model fitting, a cross validation method was used with five evaluation indices: the mean standardized error was close to 0, the root mean square was minimized, the mean error was close to the root mean standardized error, and the average standardized error was close to 1 (Li et al. 2013).

It was important to note that flood depth may be negative for some individual points in the edges, and it was also negative if there were small pieces of highlands unable to distinguish in the remote sensing images, which was the real reflection of the water surface elevation. In this paper, we could use the Setnull function in the Raster Calculator tool to correct the negative situation in the results of the flood depth calculation, so that the water depth results were in line with the general understanding.

Results and analysis

Spatial distribution of flood extent in ungauged basins

Macro-dynamic monitoring of inundation

The water bodies in the Jushui Basin were extracted by calculating the NDVI index of the MODIS surface reflectance productions. The extraction accuracy was verified via the Landsat-7 ETM+ image and GF-1 WFV4 data (see Table 2). On day 190 of 2016, i.e., on July 8, it was 91.79%, and it was 98.5% on day 191, i.e., on July 9. The actual accuracies with high accuracy data as standard were 92.20 and 98.17%, respectively. Therefore, this method achieved good results and could be used as a basis for judging the NDVI threshold in the water extraction by MODIS.

The macro-dynamic monitoring of flood inundation in the Jushui Basin was showed in Fig. 3. Some M

ODIS images were not showed for their unavailability due to serious cloud coverage. The inundation condition from different sources had consistency in spatial distribution, even though the profiles of the DFO flood database were a little smaller. The flooded areas were primarily concentrated near the junction of the Jushui and Shahe Rivers, the area between the Qingcao and Zhanjia Lakes, and the bend in the river channel in the

southwest, all of which were located in Tuanfeng. The reason for this phenomenon is that the topography of the basin slopes from northeast to southwest, with a large difference in terrain. The low hilly land and lake on the plains are located in the northeast and southwest regions of Tuanfeng, respectively. The Qingcao Lake is the lowest point with an elevation of only 15.8 m above sea level. After a strong rainfall, flood water converges in low-lying areas. Therefore, as a tributary, the Shahe River constantly flows into the Jushui River, which leads to rapid increases in the water level during the rainfall event, and forms inundation. The Yellow Lake community is located between the Qingcao and Zhanjia Lakes and is densely populated with more impervious surfaces. Therefore, it is easy to form waterlogging there when floods occur. According to news reports, due to the long-term rainwater immersion, the Jushui River burst next to the Yellow Lake community at 3 am on July 5, validating the above result. As for the bend in the river channel in the southwest, because the river was in a bend state, flood water could not move along the river channel at high speeds and rushed out of the river bank under the inertial force, submerging the shore on both sides.

Spatial change monitoring of flood extent

The MODIS surface reflectance productions and the DFO flood database were only suitable for macro-dynamic monitoring of inundation for their low resolution, so they could not reflect the spatial changes in the flood extent and inundation features during the flood period. This paper used a GF-1 WFV3 image that provided the background water bodies in the Jushui Basin, Landsat-7 ETM+ image, GF-1 WFV4 data, and Sentinel-1 SAR data to calculate flood extent in order to understand their spatial changes (see Fig. 4). As could be seen, the flood extent on July 5 was the largest and river channel in the lower reaches of the Jushui Basin was significantly widened, with many small flooding plaques. The inundated area was primarily concentrated at the junction of the Jushui and Shahe Rivers, the area between the Qingcao and Zhanjia Lakes, and the bend in the river channel in the southwest, consistent with the above analysis. The river water and the flood water flowed into the Qingcao and Zhanjia Lakes, expanding the coverage of the flood. As a tributary, the Shahe River also presented significant changes. From July 8 to July 9, the flood extent changed little, but inundation was still severe compared to the background water. Therefore, in

Table 2 Verification of the water extraction accuracy in the Jushui Basin

Time series	Data source	Resolution	Unit area (hm ²)	Pixel number	Water area (hm ²)	Accuracy (15/16 m standard)	Accuracy (250 m standard)
190	ETM+	15 m	0.0225	230,754	5191.96		
190	ETM+ transition	250 m	6.25	827	5168.75		
190	MODIS	250 m	6.25	901	5631.25	92.20%	91.79%
191	WFV4	16 m	0.0256	214,625	5494.4		
191	WFV4 transition	250 m	6.25	850	5312.5		
191	MODIS	250 m	6.25	863	5393.75	98.17%	98.5%

order to carry out relief measures scientifically, government should increase preventative measures at the junction of the Jushui and Shahe Rivers and take appropriate measures to deal with the situation. With respect to the distribution of emergency relief materials, we should pay more attention to residential areas in order to protect the needs of the victims and to reduce casualties.

According to the comprehensive information in Figs. 3 and 4, the evolution process of flood water in the Jushui Basin was divided into three periods: the rising period from July 1 to July 5 during the continuous rainfall, the flood period from July 8 to July 13, and the recession period after July 14. Affected by the heavy rainfall and basin topography, the water level of the lower reaches rose and the flood extent expanded; from July 8 to July 13, the inundated area did not change apparently. The main reason was that the high water level in the Wuhan section of the Yangtze River made the water level in the Jushui River dropped gradually, then the flooding began to recede.

Spatial distribution of the flood depth in ungauged basins

The Kriging interpolation of Geostatistical Analyst in ArcGIS was used to interpolate the water surface elevation on the basis of the flood extent in the lower reaches of the Jushui Basin for obtaining a discrete distribution of the water surface elevation. Focusing on the area near the Yellow Lake community, it could be seen that the areas with higher water surface elevations were concentrated at the junction of the Jushui and Shahe Rivers, the area around the Zhanjia Lake, and the bend in the river channel in the southwest, similar to the above analysis of the flood extent (see Fig. 5). In addition, compared to other areas, the water level in these areas rose rapidly, resulting in higher water surface elevations.

By calculating the difference between the water surface elevation and the terrain elevation, the flood depth was calculated as shown in Fig. 6. The flood depth was mainly 0–2 m, and it was greater than 6 m on July 5 at the Zhanjia Lake. On July 9, the flood depth had declined. However, waterlogging remained in the Yellow Lake community because it was difficult to dredge water flow in a short time and easy to form a waterlogged status in such a place where houses were lined up. The fact that the first floors of the residential buildings were primarily garages, warehouses, and stores and that the flooding was serious, also confirmed the results.

In addition, according to the information column of the Civil Affairs Bureau of Huanggang, the rainstorm events from June 30 to July 6, 2016, in Tuanfeng affected a total of 325,400 people and resulted in a total economic loss of 1.376 billion yuan. In the early hours of July 6, the water level of the Zhanjia Lake increased by heavy rainfall and the levees broke. Floods inundated the Yellow Lake community, making it the most affected area in the county. Therefore, the Yellow Lake community and the lake were indeed flooded, which validated the above analysis. According to water level data provided by the official website of the Bureau of Hydrology and Water Resources in Hubei Province, the average mean water level at the Liuzi Port hydrological station on July 5 was 27.674 m, while on July 9, it was 27.103 m. Therefore, with the end of the rain, the water level began to drop and the flooding in the plains receded. Indirectly, the flood depth monitoring results were verified in this paper.

Discussion and conclusion

As a serious natural disaster, floods greatly influence human lives and social economy, which seriously

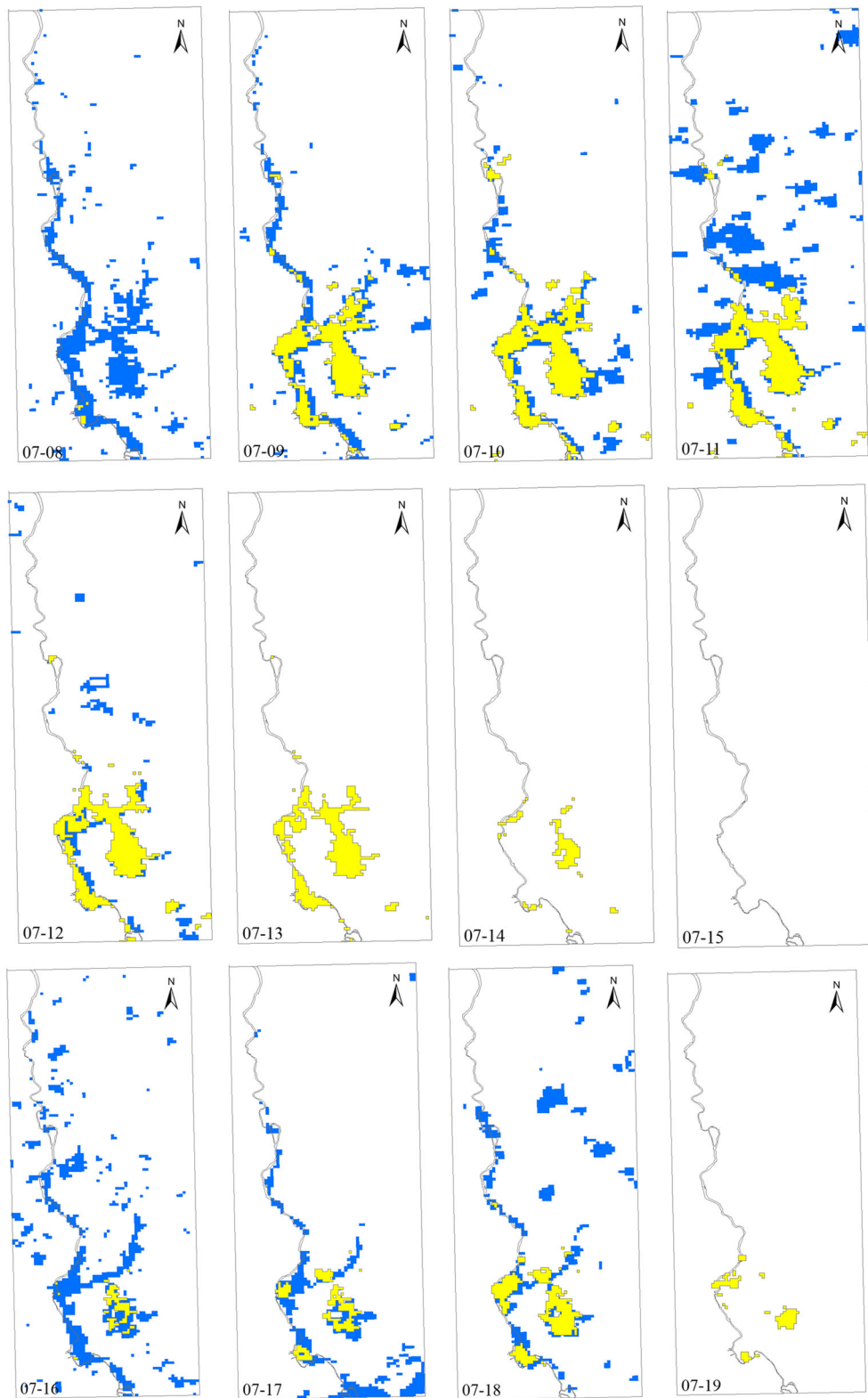


Fig. 3 Macro-dynamic monitoring of flood inundation in the lower reaches of the Jushui Basin from July 1, 2016, to July 20, 2016

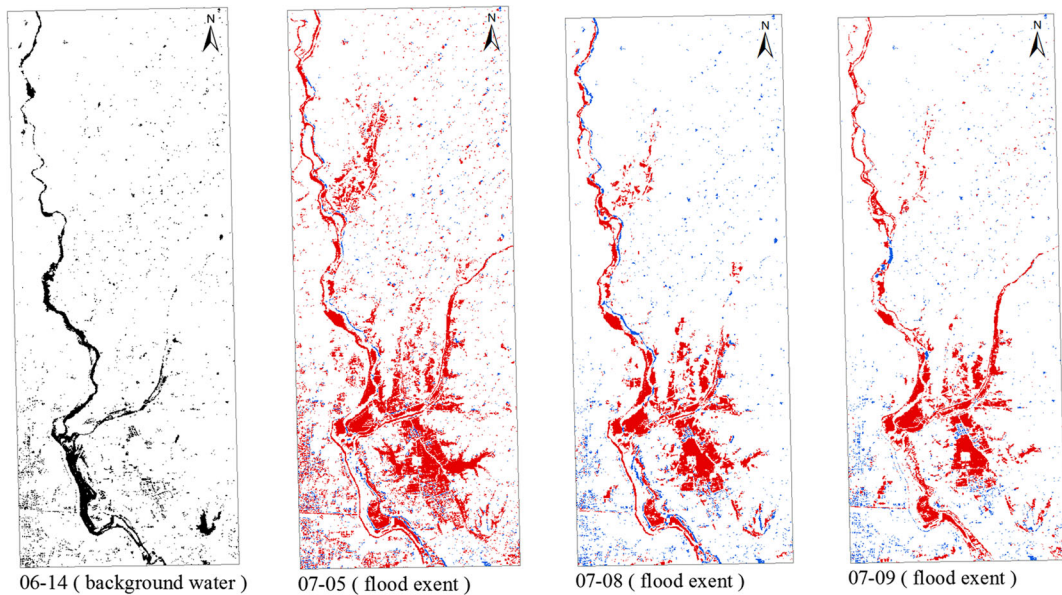


Fig. 4 Spatial distribution of the flood extent in the lower reaches of the Jushui Basin from July 5, 2016, to July 9, 2016

hinders society development in a good order and normal operation. The severe floods in Central Europe during the last decade led the European Union to set in force the new Flood Directive 2007/60 which can be characterized as an innovative paradigm for the defense against floods (Tsakiris 2014). Performing near-real-time detection with flood extent and depth based on multi-source remote sensing data in a time series, this study analyzed the inundation condition and the characteristics of flood disaster in ungauged basins. The results of this study can further promote the researches on flood detection in ungauged basins with the help of remote sensing technique, which also provides decision-making support for

governmental departments. The main conclusions are as follows:

- 1) The multi-source remote sensing data can make up the lack of hydrological data in ungauged basins, which is helpful to reconstruct hydrological sequence and analyze flood inundation.
- 2) The combination of MODIS surface reflectance productions and the DFO flood database can achieve the macro-dynamic monitoring of the inundation in ungauged basins, and then the differential technique of high-resolution optical and microwave images before and after floods can be used to

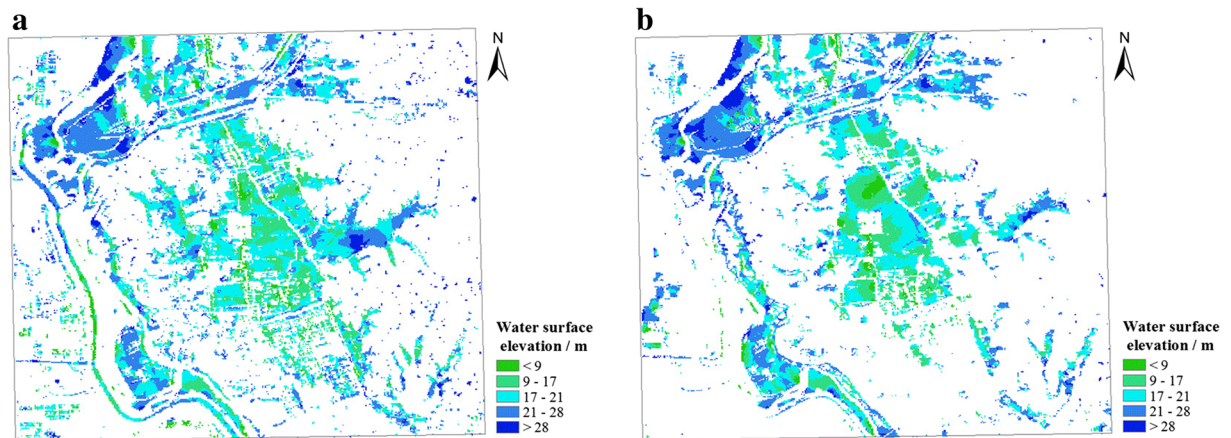


Fig. 5 Spatial distribution of the water surface elevation in the lower reaches of the Jushui Basin. **a** On July 5 and **b** on July 9

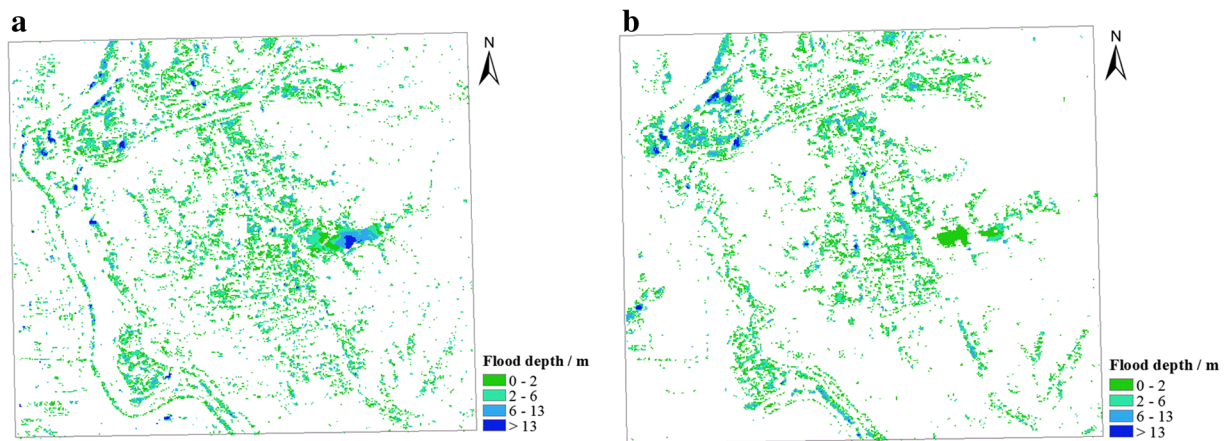


Fig. 6 Spatial distribution of the flood depth in the lower reaches of the Jushui Basin. **a** On July 5 and **b** on July 9

calculate flood extent to reflect spatial change of inundation.

- 3) The monitoring algorithm for the flood depth combining RS and GIS is simple and easy and can quickly calculate the depth with a known flood extent that is obtained from remote sensing images in ungauged basins. In this process, the Kriging method in the Geostatistical Analyst can verify the accuracy of the interpolation for the water surface elevation, which makes up the shortage of the field validation.

Overall, the near-real-time detection with flood extent and depth reflects the spatial-temporal variation characteristics and development of floods in ungauged basins, so it is a feasible method to monitor floods when the study area is located outside the hydrological monitoring network. However, this paper has to be improved, because it still has several limitations, such as the direct use of the NDVI index for water extraction in the Jushui Basin, without a comparison between the water extraction indices and the set of NDVI index threshold. The mixed pixel processing also contains some subjectivity and requires a more accurate water extraction model. In addition, due to the relatively low spatial resolution of the profiles provided by the DFO flood database, some small flood disasters are not well monitored. Further, the Kriging interpolation accuracy is affected by the accuracy of the DEM data types, the distribution of boundary point, interpolation method, and so on. These problems will be explored in following studies.

Funding information This research is supported by the National Key Basic Research Program of China (2013CB430200 (2013CB430206)) and the China Special Fund for Meteorological Research in the Public Interest (GYHY201306056).

References

- Ahamed, A., & Bolten, J. D. (2017). A MODIS-based automated flood monitoring system for southeast asia. *International Journal of Applied Earth Observation and Geoinformation*, *61*, 104–117. <https://doi.org/10.1016/j.jag.2017.05.006>
- Aronica, G. T., Candela, A., Fabio, P., & Santoro, M. (2012). Estimation of flood inundation probabilities using global hazard indexes based on hydrodynamic variables. *Physics and Chemistry of the Earth*, *42-44*, 119–129. <https://doi.org/10.1016/j.pce.2011.04.001>
- Awadallah, A. G., & Tabet, D. (2015). Estimating flooding extent at high return period for ungauged braided systems using remote sensing: a case study of Cuvelai Basin, Angola. *Natural Hazards*, *77*(1), 255–272. <https://doi.org/10.1007/s11069-015-1600-6>
- Calkoen, C. J., Hesselmann, G. H. F. M., Wensink, G. J., & Vogelzang, J. (2001). The bathymetry assessment system: efficient depth mapping in shallow seas using radar images. *International Journal of Remote Sensing*, *22*(15), 2973–2998. <https://doi.org/10.1080/01431160116928>
- Du, X. P., Guo, H. D., Fan, X. T., Zhu, J. J., Yan, Z. Z., Zhan, Q., & Sun Z. C. (2012). Flood modeling and inundation risk evaluation using remote sensing imagery in coastal zone of China. *Geoscience and Remote Sensing Symposium (IGARSS)*, 2012 I.E. International.
- Huang, S. F., Chen, D. Q., Li, X. T., Sun, T., Li, J. G., & Xu, M. (2012). *Methods and practice of remote sensing monitoring and evaluation of flood disaster*. Beijing: China Water & Power Press.
- Huang, T., Shi, Q. S., Shi, Q. D., & Anayet, A. (2013). Validate classification precision of low spatial resolution remote

- sensing data by using high spatial resolution data. *Journal of Xinjiang University*, 30(2), 238–242.
- Huang, C., Chen, Y., & Wu, J. P. (2014). Mapping spatio-temporal flood inundation dynamics at large river basin scale using time-series flow data and MODIS imagery. *International Journal of Applied Earth Observation and Geoinformation*, 26, 350–362. <https://doi.org/10.1016/j.jag.2013.09.002>
- Huang, X. D., Wang, J. F., & Shang, J. L. (2016). An adaptive two-component model-based decomposition on soil moisture estimation for C-band RADARSAT-2 imagery over agricultural fields. *Geoscience and Remote Sensing Letters, IEEE*, 13(3), 414–418.
- Khan, S. I., Hong, Y., Wang, J. H., Yilmaz, K. K., Gourley, J. J., Adler, R. F., Brakenridge, G. R., Policelli, F., Habib, S., & Irwin, D. (2011). Satellite remote sensing and hydrologic modeling for flood inundation mapping in Lake Victoria Basin: implications for hydrologic prediction in ungauged basins. *IEEE Transactions on Geoscience and Remote Sensing*, 49(1), 85–95. <https://doi.org/10.1109/TGRS.2010.2057513>
- Li, J. X., Li, C. K., & Yin, Z. H. (2013). ArcGIS based on Kriging interpolation method and its application. *Bulletin of Surveying and Mapping*, 9, 87–90.
- Li, J. L., Cao, L. D., & Pu, R. L. (2014). Progresses on monitoring and assessment of flood disaster in remote sensing. *Shuili Xuebao*, 45(3), 253–260.
- Liang, L., Di, L. P., Zhang, L. P., Deng, M. X., Qin, Z. H., Zhao, S. H., & Lin, H. (2015). Estimation of crop LAI using hyperspectral vegetation indices and a hybrid inversion method. *Remote Sensing of Environment*, 165(8), 123–134. <https://doi.org/10.1016/j.rse.2015.04.032>
- Liang, L., Qin, Z. H., Zhao, S. H., Di, L. P., Zhang, C., Deng, M. X., Lin, H., Zhang, L. P., Wang, L. J., & Liu, Z. X. (2016). Estimating crop chlorophyll content with hyperspectral vegetation indices and the hybrid inversion method. *International Journal of Remote Sensing*, 37(13), 2923–2949. <https://doi.org/10.1080/01431161.2016.1186850>
- Liu, M. L., Tang, X. M., & Liu, J. Y. (2001). Research on scaling effect based on 1km grid cell data. *Journal of Remote Sensing*, 5(3), 183–190.
- Matgen, P., Schumann, G., Henry, J. B., Hoffmann, L., & Pfister, L. (2007). Integration of SAR-derived river inundation areas, high-precision topographic data and a river flow model toward near real-time flood management. *International Journal of Applied Earth Observation and Geoinformation*, 9(3), 247–263. <https://doi.org/10.1016/j.jag.2006.03.003>
- McFeeters, S. K. (1996). The use of the normalized difference water index (NDWI) in the delineation of open water features. *International Journal of Remote Sensing*, 17(7), 1425–1432. <https://doi.org/10.1080/01431169608948714>
- Nakmuenvai, P., Yamazaki, F., & Liu, W. (2017). Automated extraction of inundated areas from multi-temporal dual-polarization RADARSAT-2 images of the 2011 central Thailand flood. *Remote Sensing*, 9(1), 78. <https://doi.org/10.3390/rs9010078>
- Nigro, J., Slayback, D., Policelli, F., & Brakenridge, G. R. (2014). NASA/DFO MODIS near real-time (NRT) global flood mapping product evaluation of flood and permanent water detection.
- Papa, F., Prigent, C., & Rossow, W. B. (2008). Monitoring flood and discharge variations in the large Siberian rivers from a multi-satellite technique. *Surveys in Geophysics*, 29(4-5), 297–317. <https://doi.org/10.1007/s10712-008-9036-0>
- Plate, E. J. (2002). Flood risk and flood management. *Journal of Hydrology*, 267(1-2), 2–11. [https://doi.org/10.1016/S0022-1694\(02\)00135-X](https://doi.org/10.1016/S0022-1694(02)00135-X)
- Powell, S. J., Jakeman, A., & Croke, B. (2014). Can NDVI response indicate the effective flood extent in macrophyte dominated floodplain wetlands? *Ecological Indicators*, 45, 486–493. <https://doi.org/10.1016/j.ecolind.2014.05.009>
- Qian, X. J., Liang, L., Shen, Q., Sun, Q., Zhang, L. P., Liu, Z. X., Zhao, S. H., & Qin, Z. H. (2016). Drought trends based on the VCI and its correlation with climate factors in the agricultural areas of china from 1982 to 2010. *Environmental Monitoring and Assessment*, 188(11), 639. <https://doi.org/10.1007/s10661-016-5657-9>
- Sandridge, J. C., & Holyer, R. J. (1998). Coastal bathymetry from hyperspectral observations of water radiance. *Remote Sensing of Environment*, 65(3), 341–352. [https://doi.org/10.1016/S0034-4257\(98\)00043-1](https://doi.org/10.1016/S0034-4257(98)00043-1)
- Shen, Q., Liang, L., Luo, X., Li, Y. J., & Zhang, L. P. (2017). Analysis of the spatial-temporal variation characteristics of vegetative drought and its relationship with meteorological factors in China from 1982 to 2010. *Environmental Monitoring and Assessment*, 189(9), 471. <https://doi.org/10.1007/s10661-017-6187-9>
- Tsakiris, G. (2014). Flood risk assessment: concepts, modelling, applications. *Natural Hazards and Earth System Science*, 2, 261–286.
- Wolski, P., Murray-Hudson, M., Thito, K., & Cassidy, L. (2017). Keeping it simple: monitoring flood extent in large data-poor wetlands using MODIS SWIR data. *International Journal of Applied Earth Observation and Geoinformation*, 57, 224–234. <https://doi.org/10.1016/j.jag.2017.01.005>
- Xu, H. Q. (2006). Modification of normalised difference water index (NDWI) to enhance open water features in remotely sensed imagery. *International Journal of Remote Sensing*, 27(14), 3025–3033. <https://doi.org/10.1080/01431160600589179>
- Yi, Y. H., Chen, X. W., & Wu, H. (2005). An algorithm for inundated depth calculation of flood based on remotely sensed data. *Geography and Geo-Information Science*, 21(3), 26–29.
- Zeng, L. F., Li, L., & Wang, L. H. (2015). SAR-based fast flood mapping using Sentinel-1 imagery. *Geomatics World*, 22(5), 100–107.
- Zhang, Q. X., & Wang, Y. C. (2009). Development and application of two dimensional unsteady flood routing model. *Water resources and Hydropower Engineering*, 40(3), 62–65.
- Zhang, H. B., Li, J. S., Xiang, N. P., Shen, Q., & Zhang, F. F. (2015). A study of extracting water bodies automatically based on the MODIS surface reflectance data. *Remote Sensing Technology and Application*, 30(6), 1160–1167.
- Zhao, S. L., Wang, J. P., & Wang, Y. F. (2016). A research on defining the water depth in Cuochuolong Lake retrieval from OLI image. *Journal of Salt Lake Research*, 24(1), 8–14.
- Zwenzner, H., & Voigt, S. (2009). Improved estimation of flood parameters by combining space based SAR data with very high resolution digital elevation data. *Hydrology and Earth System Sciences*, 13(5), 567–576. <https://doi.org/10.5194/hess-13-567-2009>